New CBP derivatives with locked carbazole-biphenyl junctions – high triplet state energy materials

Journal:	*Chemistry of Materials*
Manuscript ID:	cm-2014-045754.R1
Manuscript Type:	Article
Date Submitted by the Author:	03-Feb-2015
Complete List of Authors:	Gantenbein, Markus; University of Basel, Department of Chemistry Hellstern, Manuel; University of Basel, Department of Chemistry Le Pleux, Loic; University of Basel, Department of Chemistry Neuburger, Markus; University of Basel, Department of Chemistry Mayor, Marcel; University of Basel, Department of Chemistry; Karlsruhe Institute of Technology (KIT), Institute of Nanotechnology (INT)

New CBP derivatives with locked carbazole-biphenyl junctions – high triplet state energy materials

Markus Gantenbein, Manuel Hellstern, Loïc Le Pleux, Markus Neuburger, Marcel Mayor

Abstract

We synthesized a series of **CBP** derivatives, using methyl groups as spatially demanding groups, locking the angle between the carbazole subunit and the biphenyl backbone as potential matrix material for blue organic light emitting diodes (OLEDs). The locked rotation was achieved by four methyl groups either in the 1,8-positions of the carbazole subunit (**1**) or in the 3,5,3',5'-positions of the biphenyl subunit (**2**) and the fixed spatial arrangement was confirmed by x-ray analysis. The physical properties of **CBP** derivatives based on the parent structure **2** were further tailored by electron withdrawing CF_3-groups in 3,6- or 2,7-positions of the carbazole subunits (**3** and **4**) or alternatively by electron donating CH_3O-groups in the 2,7-positions (**5**) of the same building blocks. Increased triplet energies (E_T) compared to the parent compound **CBP** were found for all synthesized **CBP** derivatives **1**-**5**. Enhanced glass transition temperatures ranging between 129°C to 205°C further corroborate the application potential of these derivatives for matrix material in blue emitting OLEDs.

Introduction

The potential of cheap solar cells, organic field-effect transistors, and organic light-emitting diodes (OLEDs) is fueling the interest in research on organic materials. The performance of such devices critically depends on the efficiency in which charge carriers (holes and electrons) move within π-conjugated materials. For the development of efficient π-conjugated materials, a profound understanding of the interplay between the π-electron delocalization and geometrical structural features is required.

Especially phosphorescent organic light emitting diodes (phOLEDs) have received considerable attention because unlike standard fluorescent OLEDs, which feature singlet excitons, phOLEDs are based on triplet

excitons in the emitter. Due to elementary spin statistics 75% triplet excitons and 25% singlet excitons are formed on initial charge recombination. By fast intersystem crossing all singlet excitons are efficiently converted into the triplet state and hence, the theoretical limit of the internal quantum efficiency is 100% with these phosphorescent emitters. In a typical phOLED, the emitters are usually doped with suitable host materials for reducing concentration quenching and triplet–triplet annihilation.

To maximize phOLED efficiency a high performing host molecule needs to fulfill the following criteria: (i) the triplet energy (E_T) of the host molecule should be higher than the corresponding one of the phosphorescent guest emitter, to prevent the back energy transfer from guest to host and to promote the exothermic energy transfer from host to guest, (ii) facile and balanced charge injection from neighboring layers, and (iii) HOMO and LUMO levels of the host molecules should be appropriately aligned with the hole transport layer (HTL) and electron transport layer (ETL) to reduce the driving voltage for charge injection. The use of high-E_T materials is imperative to confine the triplet excitons in the emitter. In blue phosphorescent OLEDs in particular, a host material with a high E_T of over 2.75 eV is required. Due to its triplet energy ΔE (T_1–S_0) of 2.56 eV, 4,4'-Bis(9-carbazolyl)-biphenyl (**CBP**) is a suitable matrix for green phosphorescent emitters like tris(2-phenylpyridine)iridium(III) (**Ir(ppy)$_3$**). Blue emitting materials such as the commonly used bis((4,6-difluorophenyl)-pyridinato-N,C2)picolinate-iridium(III) (**FIrpic**) (ΔE (T_1–S_0) = 2.65 eV) require hosts with higher triplet energies. The key to obtain such high E_T materials is to confine the conjugated system within the host molecules.[1]

By variation of the torsion angle Φ between the planes of the two phenyl rings of biphenyl derivatives, we have previously reported that the degree of π-overlap in the two phenyl rings and the resulting extent of delocalization over both π-systems can be fine-tuned.[2] In most cases this tuning is performed by substituting biaryls in the 2 and 2' position with different sterically demanding groups or by interlinking the two positions with alkyl chains of different lengths. This approach, which aim to increase the triplet energy of **CBP** based materials by reducing the extent of conjugation in the biphenyl scaffold is currently thoroughly studied and was recently reviewed in details by Yang and co-workers.[1,3] Tokito and co-workers reported the new host 4,4'-bis(9-carbazolyl)-2,2'-dimethylbiphenyl (**CDBP**) with a high E_T of 2.79 – 3.0 eV (the reported values differ within this range) by introducing two methyl groups in 2- and 2'-positions of biphenyl in CBP structure.[4] Strohriegl and co-workers modified the **CDBP** structure by introducing CF_3 groups instead of CH_3 groups on the biphenyl core, while investigating the influence of the substitution on the 3,6-positions of the carbazole. This leads not only to a loss of conjugation in the central biphenyl core but also to high triplet energies.[5,6]

Here we are less interested in the interphenyl angle of the biphenyl backbone. Instead we report here compounds which were synthesized to investigate correlations between their physical properties and the spatial arrangement between biphenyl and carbazole subunits. The molecular design is based on the idea that reducing the conjugation between the subunits gives molecules which display optical features of their individual subunits, with the whole molecule being able to form amorphous molecular materials. In this context we have prepared a series of **CBP** derivatives with sterically restricted degrees of freedom in their biphenyl-N-carbazole junctions, due to substituents either in the 1,8-positions of the carbazole subunit (**1**) or in the 3,5,3',5'-positions of the biphenyl subunit (**2**). In the latter case the electronic features of the carbazole synthons were further varied by substituents either in the 3,6- or in the 2,7-positions (Figure 1). We report here the synthesis of five amorphous **CBP** derivatives together with their thermal and optical properties. The energy levels have been measured by electrochemical measurements and optical spectroscopy techniques. Additional insights into geometrical features of the **CBP** derivatives were obtained by analyzing their solid state structures by x-ray diffraction analysis and with DFT calculations.

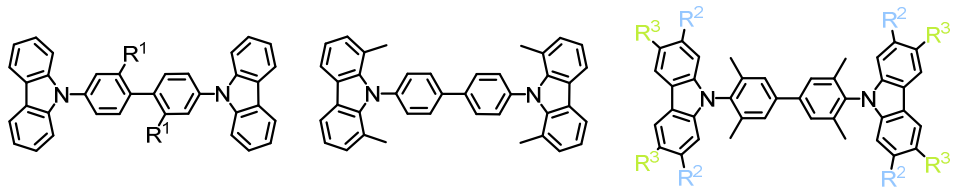

CBP: $R^1 = H$
CDBP: $R^1 = CH_3$

1

2: $R^2 = R^3 = H$
3: $R^2 = H$, $R^3 = CF_3$
4: $R^2 = CF_3$, $R^3 = H$
5: $R^2 = OCH_3$, $R^3 = H$

Figure 1: Chemical structures of the CBP derivatives 1-5

Results and discussion

Synthesis

Scheme 1: Synthesis and molecular structure of rotational restricted CBP derivatives 1a and 1b.

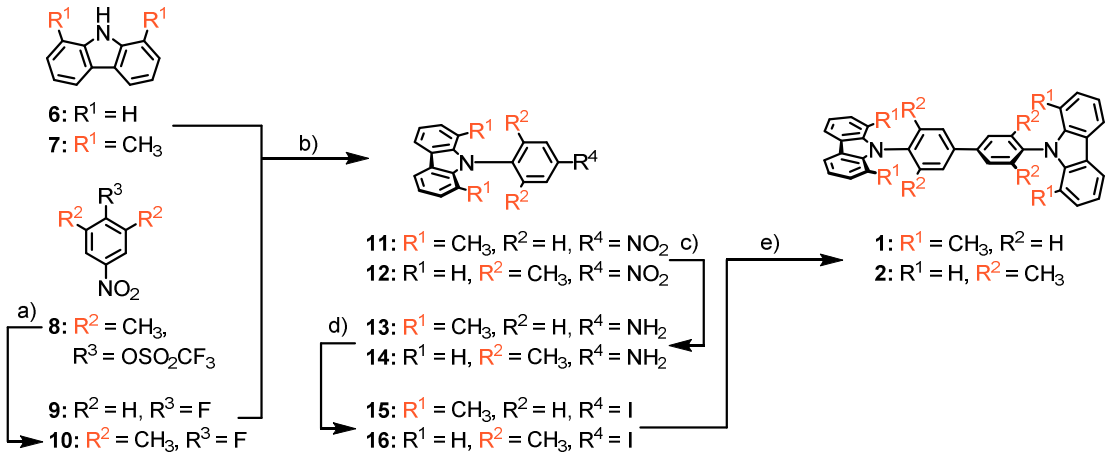

[a]Reaction conditions: a) $[(cinnamyl)_2Pd])_2$ (2.5 mol%), ^{t}BuBrettPhos (7 mol%), CsF, MePh, 110°C, 24h, 93%; b) Cs_2CO_3, DMF, 12h, 150°C, **11** (86%), **12** (87%), c) $SnCl_2 \cdot 2H_2O$, EtOH, reflux, 4h, **13** (91%), **14** (94%); d) BF_3 Et_2O, ^{t}BuONO, THF, KI, I_2, MeCN, -10°C to rt, 12h, **15** (75%), **16** (79%); e) Turbo Grignard, TEMPO, THF, -10°C to rt , 2h, **1** (96%), **2** (97%).

Carbazole **7** was synthesized according to literature[7] in a one pot Pd - catalyzed Buchwald-Hartwig amination followed by C-H activation procedure, whereas carbazole (**6**) was commercially available. Fluoro-nitro compound **10** was synthesized starting from the commercially available 2,6-dimethyl-4-nitro phenol. The phenolic alcohol was transformed into the triflate **8** using triflic anhydride and pyridine. According to a procedure reported by Buchwald and co-workers, a Pd - catalyzed fluorine insertion replacing the triflate moiety was used to provide the fluoro-nitro compound **10** in multigram scale[8]. The 9-*para*-nitrophenylcarbazole compounds **11**-**12** were synthesized *via* an aromatic nucleophilic substitution reaction (S_NAr)[9,10] between the carbazoles (**6** or **7**) and the *para*-fluoronitrobenzene derivatives (**9** or **10**), using Cs_2CO_3 in DMF at reflux temperature. First attempts based on Buchwald-Hartwig[11] or Ullmann conditions[12] did not lead to the desired conversion, what we attributed to steric factors. Reduction of the nitro groups of **11**-**12** with tin chloride[13] afforded the anilines **13**-**14**, which were transformed directly to the corresponding aryl iodide compounds **15**-**16** *via* Sandmeyer reactions.[14] The homo-coupling of the aryl iodide derivatives provided the desired **CBP** derivatives **1** and **2**. The reaction conditions for the homo-coupling were optimized by preliminary screening experiments. Copper catalyzed reaction conditions like classical Ullmann conditions,[12]

alternative $Cu^{(I)}$ sources,[15] also including immobilized $Cu^{(II)}$ sources[16] did not provide the desired **CBP** derivatives in reasonable yields. To our delight, Knochel's Turbo Grignard reaction[17] conditions in combination with TEMPO[18] as co-oxidant provided the desired target **CBP** derivatives **1** and **2** in excellent yields of 96% and 97%, respectively. Both target structures **1** and **2** were fully characterized by ^{1}H- and ^{13}C-NMR spectroscopy, mass spectrometry (MS), and elemental analysis. In addition optical and electronic properties of these structures have been analyzed and will be discussed below. An important finding of these studies is mentioned already here, as it steered the molecular design and thus also the evolution of our experimental approach. Comparing **1** and **2** we don't find big differences in their optical properties and thus we conclude, that the methyl groups sterically locking the spatial arrangement of the phenyl-carbazole junction are equally efficient whether they are mounted at the carbazole (**1**) or at the biphenyl subunit (**2**). We thus decided to maintain with the methyl groups at the biphenyl backbone and to profit from the not yet functionalized carbazole subunits to introduce substituents in order to tune the physical properties of the **CBP** derivatives. The decision to favor analogs of **2** over the ones of **1** was also chemically encouraged by the relatively poor solubility and the challenging synthesis of **1**.

Scheme 2: Synthesis and molecular structure of CBP derivatives 3-5, as carbazole functionalized analogs of 2.

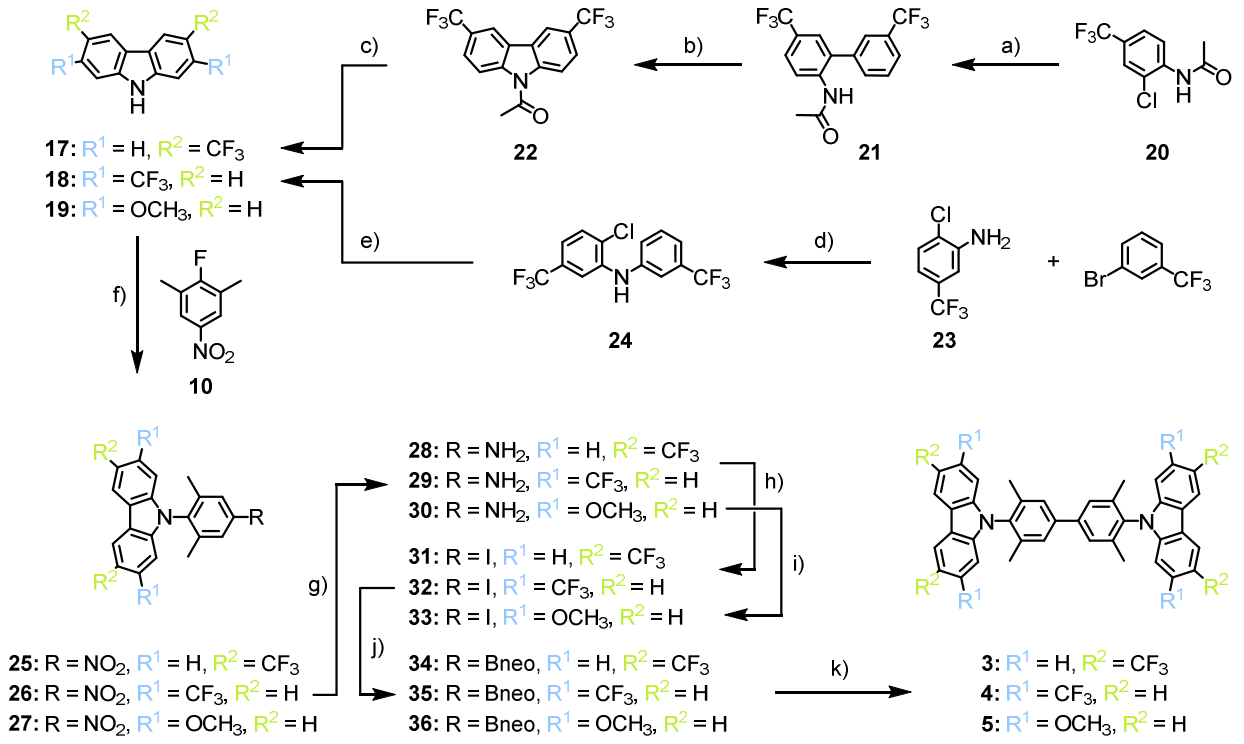

Reaction conditions: a) SPhos Pd G2 (2 mol%), 3-(Trifluoromethyl)phenylboronic acid, K_3PO_4, THF : H_2O (20:1), 80°C, 12h, 93%; b) $Pd(OAc)_2$ (2mol%), $Cu(OAc)_2$ (20 mol%), MePh, 120°C, 24h, 98%; c) H_2SO_4 :

MeOH (1:5), 80°C, 0.5h, quant; d) $Pd_2(dba)_3$, BINAP, NaO^tBu, MePh, 90°C, 12h, 93%; e) NaO^tBu, $HPtBu_3][BF_4]$, $Pd(OAc)_2$, MePh, 160°C (MW), 3h, 81%; f) Cs_2CO_3, DMF, 12h, 150°C, **25** (82%), **26** (78%), **27** (86%); g) $SnCl_2 \cdot 2H_2O$, EtOH, reflux, 4h, **28** (92%), **29** (93%), **30** (97)%; h) $BF_3 \cdot Et_2O$, ^tBuONO, DCM, KI, I_2, -10°C - rt, 12h, **31** (82%), **32** (90%); i) PTSA, $NaNO_2$, KI, MeCN, H_2O, 10°C, 2h, **33** (83%); j) Turbo Grignard, $B(O^iPr)_3$, neopentyl glycol, THF, -10°C to rt, 12h; k) SPhos Pd G2 (2 mol%), K_3PO_4, THF : H_2O (20:1), 60°C, 12h, **3** (95%), **4** (93%), **5** (97%) over 2 steps.

To apply the assembly strategy displayed above for **2**, the substituted carbazoles **17**-**19** were required. Carbazole **17** was synthesized by analogy to a literature procedure.[19] Commercially available 2-chloro-4-(trifluoromethyl)aniline was acetylated using acetyl chloride and pyridine yielding **20**. The biphenyl **21** was obtained in very good 93% yield using a Suzuki-Miyaura cross-coupling protocol. The acetylated carbazole **22** was formed *via* C-H-activation. Subsequent deprotection in a solvent mixture of sulfuric acid in methanol gave the desired carbazole derivative **17** in excellent yield. Carbazole **18** was synthesized in a two-step reaction. Initial attempts bases on a Buchwald-Hartwig reaction followed by an *in-situ* C-H activation step[7] gave mixtures of compounds with very similar polarities in all reaction conditions investigated. The applied stepwise reaction protocol yielded carbazole **18** in very good yield and in gram scale. First a Buchwald-Hartwig reaction between the aniline **23** and the commercially available 1-bromo-3-(trifluoromethyl)benzene was performed to assemble the diarylamine **24**. The reaction turned out to be very sensitive to temperature with the competitive amination of the chloroaryl **23** at temperatures above 80°C. For the stepwise reaction amine **24** was filtered through a short silica plug and was used without further purification. Subsequently the carbazole was formed by ring closing C-H activation yielding **18** in 81% over both steps. The 2,7-dimethoxy carbazole **19** was synthesized following a reported procedure.[20] With the carbazoles **17**-**19** in hands, we followed the synthetic strategy described above for the synthesis of **2** as closely as possible. Namely the carbazoles were coupled in a S_NAr reaction with the fluoroaryl **10**, providing the 9-*para*-nitrophenylcarbazole derivatives **25**-**27** in good yields around 80%. Subsequently the nitro groups were reduced to the amines **28**-**30**,[13] which were exposed to a Sandmeyer[14] reaction to provide the corresponding 9-*para*-iodophenylcarbazole derivatives. While the conditions used above for **16** were successful for **31** and **32**, they failed in the case of **30**. Most likely the BF_3 etherate attacks the methoxy group resulting in the liberation of phenolic substituents. Alternatively reaction conditions developed by Knochel and co-workers[21] were applied and provided the 9-*para*-iodophenylcarbazole compound **33** in good yields (83%). The homo-coupling conditions developed above for **16** were applied to the iodoaryl precursors

31-**33**. While in the case of **31** and **32** the target compounds **3** and **4** were only obtained in poor yields, the method completely failed for **33**. A more successful synthetic approach was to first transfer the 9-*para*-iodophenylcarbazole derivatives **31**-**33** to the boronic ester derivatives **34**-**36**,[22] which were exposed without purification to Suzuki-Miyaura cross-coupling reaction conditions together with equimolar amounts of their iodoaryl precursors **31**-**33**. The target **CBP** derivatives **3**-**5** were isolated in excellent yields of 93%, 91%, and 94% respectively.

The target **CBP** derivatives **3**-**5** and their precursors were fully characterized by ^{1}H- and ^{13}C-NMR spectroscopy, mass spectrometry (MS), and elemental analysis. The identity of the **CBP** derivatives **2**-**4** was further corroborated by their solid state structures obtained by x-ray diffraction of suitable single crystals. Optical and electronic properties of the target compounds will be discussed in the course of this paper.

Thermal properties

To investigate the thermal properties of the presented **CBP** derivatives **1**-**5** differential scanning calorimetry (DSC) measurements of all compounds were performed. Measurements were recorded on a Perkin Elmer DSC Advanced Double-Furnace 8000 using scanning rates of 10 °C min^{-1}, and the glass transition temperature (T_g), crystallization temperature (T_c) and melting point (T_m) were obtained from the second heating scan. The properties of the parent **CBP** were also recorded to calibrate the experimental set-up and its recorded T_m, T_c and T_g values are in very good agreement with the literature.[6,23] Compound **2** remains in the amorphous state until 129°C, which is already twice as high as for parent compound **CBP**, whereas no T_g value could be determined for compound **1**. Furthermore, the functionalized carbazole compounds **4** and **5** showed even higher T_g values of 158°C and 184°C, respectively. Compound **3** reveals a T_g value of 202 °C, which is to the best of our knowledge, one of the highest reported value for matrix compounds. Since there is no clear trend observed for electron withdrawing or electron donating groups, we attribute these high glass transition temperatures to the decreased crystallization probability of the compounds **1-5**, due to the spatial demanding methyl groups and the functional groups attached to the carbazole subunit. By analysis of the T_m values of target compounds **1-5**, a similar T_m 351°C and 348°C has been observed for compound **1** and **3**, respectively. **4** also shows a high T_m of 314°C, whereas the compounds **2** and **5** revealed a slightly lower T_m value of 293°C and 299°C. Since the heating cycles were repeated three times starting from 20°C ending at 450°C, for all compounds **1-5** high thermal stability can be attributed. This improved thermal stability is

important for their potential application in devices like e.g. phOLEDs. Melting point, crystallization and glass transition temperature of all carbazoles **1**-**5** are summarized in Table 1. The traces of the second heating and cooling scan are presented in the supporting information (Figure S81 to S85).

Compound	Melting point[b], T_m (°C)	Crystallization temperature[b], T_c (°C)	Glass transition temperature[b], T_g (°C)
CBP[a]	288; 283 lit.	196; 205 lit.	66; 62 lit.
1	351	246	-
2	293	236	129
3	348	289	202
4	314	199	158
5	299	196	184

Table 1: [a]CBP values are in good agreement with the literature[6,23]; [b]Melting point, crystallization temperature and glass transition temperature were obtained from the second heating/cooling scan using a scan rate of 10 °C min^{-1}.

X-ray Crystallography

Single crystals, suitable for x-ray diffraction analysis, were obtained for **2**, **3** and **4** using slow evaporation techniques dissolving the compounds in a 1:1 mixture of DCM and cyclohexane. The obtained solid state structures enable the investigation of the substituents' effects on the spatial arrangement of the subunits in the solid state. Experimental details have been summarized in the supporting information (Figures S86 to S88) for all x-ray structures, which are discussed in this section. A particular focus is set on the two inter-plane twist angles between the biphenyl and the carbazole subunit (α: between green and orange plane; β: between blue and grey plane; Figure 2) and their influence on the physical properties of the **CBP** derivative. In addition the molecular structures of compounds **1**, **2** and **5** were calculated using density functional theory (DFT) calculations using B3LYP hybrid functional theory with 6-31G* basis set in Spartan10. Even though the comparability of the obtained twist angles is to some extent questionable as in the x-ray structures effects of intermolecular packing are considered as well, the calculated molecular structures provide good ideas about the spatial arrangement of their subunits.

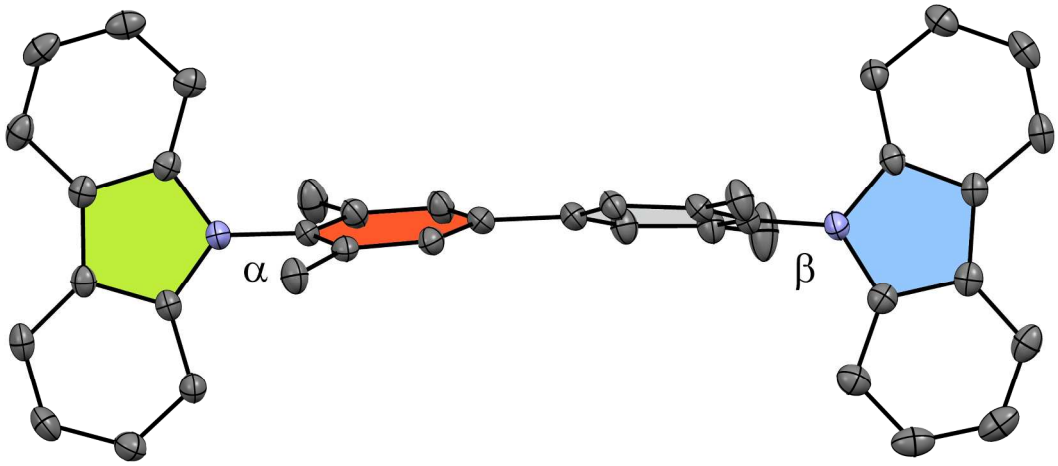

Figure 2: Solid state structure of 2. The inter-plane angle between the central carbazole ring (green) and the connected biphenyl ring (orange) is α and the one between the biphenyl (grey) and the carbazole ring (blue) is β.

Single crystal structure of compound **2** provides a non-standard monoclinic $P2_1/n$ space group and thus, the inter-plane angles α 85.05° and β 75.81° differ from each other. A similar inhomogeneity was observed in the calculations with values of 82.84° and 80.12° obtained for α and β respectively. For the **CBP** derivative **1** with the four methyl groups attached in the 1,8-positions of the carbazole subunits even increased inter-plane twist angles were calculated. With 89.96° for α and 89.93° for β, the values are very similar. Compound **3** crystallizes in the centro-symmetric orthorhombic space group *Fddd*, and

thus the inter-plane angles α and β are the same both being 88.96°. **CBP** derivative **4** crystalizes in the triclinic space group $P\bar{1}$, and its inter-plane twist angles of 79.67° for α and 76.66° for β are decreased compared to **3**. We attribute this effect to the attached CF_3-groups which are further away from the **CBP** axis in the 3,6-positions compared to the 2,7-positions. Intuitively one might thus argue that they have a bigger lever to flatten the molecule during packing in the solid state. The calculated inter-plane angles for **5** are almost perpendicular for both angles with α 89.95° and β 89.44°. For all derivatives inter-plane angles larger than 75° have been found indicating a very limited interaction between the electron clouds of neighboring aromatic subunits. In other words, the large angles break the π-electron conjugation along the molecule's axis.

Photophysical Properties

The absorption and luminescence properties of the compounds were measured in dilute and aerated dichloromethane (DCM) solution at room temperature. Figure 3 shows the corresponding UV−Vis and Emission spectra. The optical band gap of all the studied molecules were also calculated from the onset of optical absorption and are reported in Table 2.

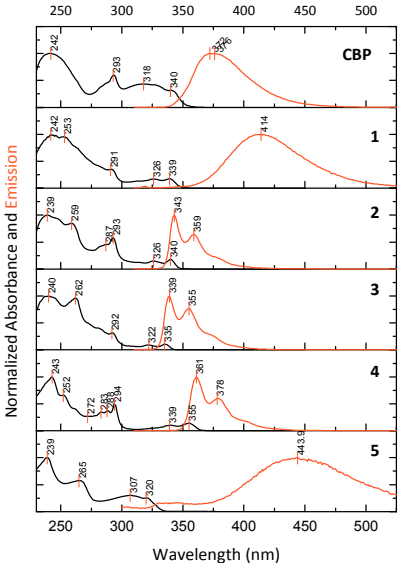

Figure 3: UV-visible and emission spectra of the compounds in DCM solution.

Table 2: Structural, photophysical and electrochemical Data

	Twist angles α/β (°)	$\lambda_{max\ uv}$ (nm)[c]	ε ($M^{-1}\cdot c^{-1}$)	$\lambda_{onset\ uv}$ (nm)[c]	E_g (eV)[d]	$\lambda_{max\ emission}$ (nm)[c]	QY (%)[c]	$\lambda_{max\ phos.}$ (nm)[e]	E_T (eV)[f]	E_{ox} vs. Fc^+/Fc (V)	E_{HOMO} (eV)	E_{LUMO} (eV)
CPB	49.5/49.5[b,24]	242 293 318 340	75380 45120 32700 23780	352	3.52	372 376	78.9	459	2.70	0.87	-5.97	-2.45
1	90.0/89.9[a]	242 253 291 326 339	102530 98460 35920 17540 18160	348	3.56	414	8.5	451	2.75	0.80	-5.90	-2.34
2	82.8/80.1[a] 85.1/75.8[b]	239 259 293 326 340	76690 64920 44660 11430 13880	347	3.57	343 359	36.9	432	2.87	0.92	-6.02	-2.45
3	89.0/89.0[b]	240 262 292 335	111570 107390 35300 12010	342	3.63	339 355	2.6	444	2.79	1.37	-6.47	-2.85
4	79.7/76.7[b]	243 294 339 355	170210 83235 17050 23830	364	3.41	361 378	15.4	420	2.95	1.36	-6.46	-3.05
5	90.0/89.5[a]	239 265 307 320	107650 61700 32500 27240	334	3.71	444	1	431	2.88	0.56	-5.66	-1.95

[a] Data from geometry optimizations at the B3LYP/6-31G* level of theory. [b] From x-ray crystal structural data. [c] All data were collected in dilute dichloromethane solution at room temperature. [d] $E_g = 1240/\lambda_{onset\ uv}$. [e] Measured in 2-MeTHF glass matrix at 77K. [f] $E_T = 1240/\lambda_{max\ phos.}$.

In order to understand how the substitutions affect the excited states of these compounds, we first consider the effect of the tetra-methyl substitution at the central biphenyl unit as well as at the 1,8-positions of both carbazoles, by comparing **1** and **2** with **CBP**.

The absorption bands at 291 nm, 326 nm and 339 nm recorded with **1** can be assigned to the absorption of the 1,8-dimethylcarbazole units. In the case of **CBP**, the features associated with transitions localized on the carbazole are present at 293 nm and 340 nm. In their fluorescence spectra **CBP** and **1** show very similar structureless emission with a maximum at 374 nm and 414 nm for **CPB** and **1** respectively. The bathochromic shift of approximately 40 nm observed in emission of **1** is caused by the additional methyl groups at the carbazole units. In the absorption spectrum of **CBP** is an additional broad absorption around 318 nm which is not observed in the case of **1**. This feature is associated with transitions between carbazole centered orbitals and orbitals localized on the biphenyl subunit and thus, the signal can be considered as a measure of conjugation between the two subunits. This band assignment and its role as conjugation indicator has been reported with comparable model compounds.[5,25,26]

The flexibility of the carbazole-biphenyl junction can not only be limited by methyl groups in the 1,8-positions of the carbazole, but alternatively by methyl groups in both *ortho*-positions of the attached phenyl ring of the biphenyl subunit as realized in **2**. Compound **2** displays almost the same carbazole centered transitions as in **CBP**, with bands localized at 293 and 340 nm. The transition between the carbazole moiety and the biphenyl core around 320 nm is weak, supporting the hypothesis of a frozen flexibility and a perpendicular arrangement of both subunits at the carbazole-biphenyl junction. In contrast to the broad emission spectrum of **CBP**, **2** exhibits a well resolved emission under identical conditions. It is obvious that inserting methyl groups on the biphenyl scaffold causes a large blue shift of the fluorescence (31 nm), caused by the decreased π-conjugation with the biphenyl core, due to a strong twist.

We now consider the effect of the di-trifluoromethane substitution at the carbazole, by comparing **2** with **3** (3,6-position) and **4** (2,7-position). The **CBP** derivative **3** displays similar carbazole centered transitions as **2** (292 and 335 nm) as well as a similar emission profile (339 and 355 nm) which is however marginally blue-shifted by 4 nm compared to **2**. In the case of **4** some of the observed transitions are red-shifted compared to **2**. In particular the second of the carbazole centered absorptions (294 and 355 nm) is bathochromically shifted by 15 nm. Even more pronounced is the 20 nm shift of the emission bands (361 and 378 nm) which, apart from the shift, display a similar pattern as the parent

structure **2**. The difference between **3** and **4** might be rationalized by an increased conjugation over both CF_3 substituents in **4**. The pioneering studies from Leclerc and co-workers comparing 3,6- with 2,7-connected polycarbazoles displayed the extended conjugation in poly-2,7-carbazole comprising a rigid poly-para-phenylene backbone compared to the poly-3,6-carbazole with a chain resembling benzidine subunits interlinked by mutual nitrogen atoms.[27] Replacing the electron withdrawing CF_3-substituents of **3** with electron donating OCH_3-groups in **5** results in blue-shifted absorption transitions (265, 320 nm). In addition a broad emission band appears at 444 nm, pointing at excited state intramolecular charge transfer (ICT) with the 3,6-dimethoxycarbazole moiety acting as the donor and the biphenyl as the acceptor.[28]

The fluorescence quantum yield (Φ_F) of those carbazole derivatives in DCM at room temperature has also been studied using a Hamamadzu Quantaurus-QY integrated sphere fluorimeter and the data are reported in Table 2. In contrast to **CBP** which shows a strong emission in those conditions, the CF_3-substituted **CBP** derivatives **3** and **4** only display low Φ_F values (0.1–0.03) suggesting an enhanced triplet yield in these derivatives.

As a prerequisite for host materials, their triplet energy should be higher than that of the phosphorescent emitter. The phosphorescence spectra of the molecules under investigation were measured in 10^{-5} M aerated and frozen 2-methyltetrahydrofuran solutions at 77 K in gated steady state conditions. The corresponding spectra are displayed in Figure 4 together with a spectrum of **CBP** for comparison. The triplet energies were determined from the highest energy peak of the phosphorescence spectra ($\lambda_{max\ phos}$) and are also listed in Table 2. The triplet energies levels are calculated according to $E_T = 1240/\lambda_{max\ phos}$.

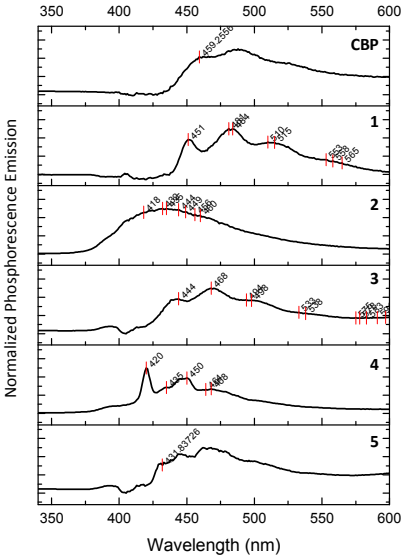

Figure 4: Phosphorescence spectra of the carbazole derivatives in 2-MeTHF glass matrix at 77K

All the synthetized **CBP** derivatives **1**-**5** show phosphorescence emission at 77 K. In spite of the broad signals the triplet energies were detectable for all five compounds and were with values between 2.75 and 2.95 eV higher than the 2.7 eV recorded for **CBP** (Figure 4). Apparently the carbazole and biphenyl subunits are efficiently decoupled by the induced twist between both in these model compounds and consequently, we can estimate that the triplet excited state in those **CBP** derivatives is mainly located on the biphenyl unit of the molecules, as substitution on the carbazole units does not affect their triplet state energy. Triplet energies of 3.1 eV for N-ethylcarbazole[29] and 2.9 eV for biphenyl (67. ± 0.6 kcal·mol^{-1})[30] corroborates this hypothesis as the triplet state will mainly be localized on the fragment with the lowest triplet energy. This hypsochromic shift of their phosphorescence makes these **CBP** derivatives with locked carbazole-biphenyl junctions interesting host materials for blue phosphorescent emitters.

In most cases exclusively fluorescence is observed in steady state conditions and phosphorescence being usually orders of magnitude weaker is difficult to observe. Here phosphorescence emission is clearly observed coexisting with fluorescence at low temperatures (see SI, figure S89 to S94). This and the decreased emission quantum yield observed at room temperature clearly points at an increase in the triplet yield of those CF_3-substituted compounds.

Electrochemical Properties

Of particular interest were the electrochemical features of these **CBP** derivatives with sterically locked carbazole-biphenyl junctions. As displayed in Figure 5 with the orbital plots of **2** the highest occupied molecular orbital (HOMO) is almost exclusively localized on the carbazole subunit while the lowest unoccupied molecular orbital (LUMO) is mainly located on the biphenyl subunit. The localization of both frontier orbitals on both decoupled subunits raised the hope that their energy levels might be tuned independently in these model compounds.

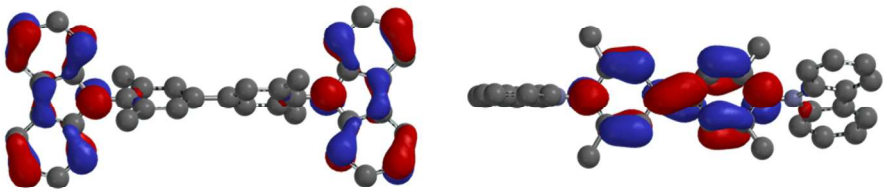

HOMO LUMO

Figure 5: Contour plots of the frontier orbitals of 2.

The oxidation potential of the **CBP** derivatives **1**-**5** were determined by DPV experiments and are summarized in Table 2. For none of the compounds a reduction process was observed within the detectable window (recorded to -2.0 V *vs*. SCE). Thus the HOMO energy levels of the compounds were estimated by their oxidation potentials after correction of the vacuum energy level (5.1 eV),[31] while the LUMO energy levels were obtained by adding the optical energy gap (E_g) obtained by absorption spectroscopy to the HOMO level ($E_{LUMO} = E_{HOMO} + E_g$). The recorded oxidation potentials are summarized in Table 2 and the determined energy levels of the frontier orbitals are depicted in Figure 6.

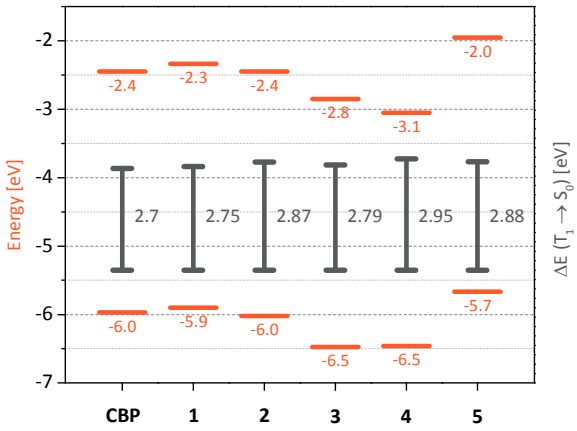

Figure 6: Energy diagram showing the position of the frontier orbital of the CBP derivatives. The dark grey line displays the position of the triplet energies.

As the HOMO of these **CBP** derivatives is mainly localized on the carbazole subunit (**Error! Reference source not found.**), the oxidation potentials of the series **2**-**5** with various carbazole substituents were particular interesting. The energy levels of the frontier orbitals of the parent structure **2** with four methyl groups at the biphenyl core are very comparable with the ones of **CBP**, while the four methyl substituents in the 1,8-postions of both carbazoles in **1** result in a slight lifting of the HOMO level due to the inductive electron donation (+I-effect) by the methyl substituents. Interestingly the LUMO of **1** is lifted by the same value in spite of the decoupling of the carbazole and the biphenyl subunits. On the other hand functionalizing the carbazole subunits with electron withdrawing CF_3-substituents (-I-effect) in **3** and **4** lower the energy level of the HOMO considerably and increase the oxidation potential by 450 mV and 440 mV respectively compared to **2**. But also in the case of **3** and **4** a similar shift of the LUMO energy level is involved, falsifying the design proposition of individually addressable energy levels of the frontier orbitals. That the HOMO level can also be lifted is displayed with **5**, in which the pronounced +I-effect of the methoxy substituents lower the oxidation potential by 360 mV compared to **2**. Also here a concomitant lifting of the LUMO is observed. In their cyclic voltammograms the **CBP** derivatives **1, 2, 4** and **5** displayed an irreversible oxidation behavior which is exemplified with **2** in Figure 7.

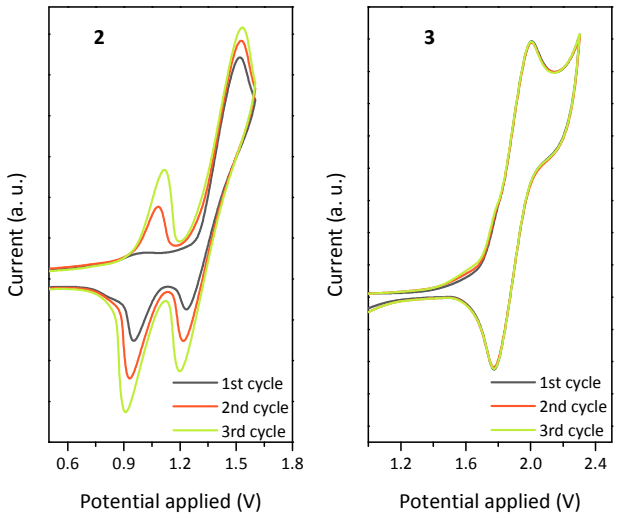

Figure 7: Cyclic voltagramm (three cycles, scan rate 100 mV/s, 10^{-3} M in DCM) of 2 (left) and 3 (right) recorded against SCE.

In the anodic scan an oxidation peak at about 1.5 V *vs.* SCE is observed which is assigned to the oxidation of the carbazole units. In the back scan not only the reduction peak between 1.2 and 1.3 V is observed, but also an additional well defined peak at about 0.9 to 1 V. It is known that after oxidation the generated radical cation is localized in the 3,6-positions of the carbazole subunit and that the proximity of radical cations at the electrode surface results in an intermolecular coupling between carbazole subunits. This dimerization is electrochemically observed as irreversible oxidation. In the subsequent scan a new oxidation peak in the region of 1.05 to 1.15 V is recorded attributed to the oxidation of the dimerization product accumulated at the Pt electrode. Similar behavior has been reported for structurally related **CBP** derivatives[5] and also for N-aryl carbazoles.[32] On the other hand, compound **3** reveals a fully reversible oxidation behavior which can be attributed to the blocking of the reactive 3,6-position of the carbazole units (Figure 7).

In summary the electrochemical studies show that the energy levels of these **CBP** derivatives can be fine-tuned to some extent by varying the substituents, and in a lesser extent by altering the substitution pattern of the pendant carbazoles. These design option is particular appealing to fine tune the energy levels of the materials involved in multilayer OLED architectures. In addition, the functionalization of the 3,6-position of the carbazole units gives electrochemically stable compounds, which would be a certain advantage as radical ions are involved in charge transport within the device.

Conclusions

A series of **CBP** derivatives with sterically locked conformation at the carbazole-biphenyl junction **1**-**5** has been synthesized and fully characterized. All **CBP** derivatives were assembled by first synthesizing the corresponding N-*para*-nitrophenyl-carbazole precursors, which were converted into N-*para*-iodophenyl derivatives, and then subsequently dimerized either by Turbo Grignard reactions or by Suzuki-Miyaura type couplings, requiring in addition the corresponding boronic acid derivatives. The key step was the nucleophilic aromatic substitution reaction (S_NAr) of the carbazole nucleophile profiting from the perfectly activated *para*-nitrofluorobenzenes, allowing to overcome the limitations of the sterically restricted reaction space at the carbazole-phenyl junctions. The rigid and almost perpendicular arrangements of the carbazole-phenyl junctions were corroborated by solid state structures of the derivatives **2**, **3** and **4**. A particular focus was set on the **CBP** derivatives with four methyl groups in the 3,5,3',5'-positions of the central biphenyl core **2**-**5**, enabling to fine tune the physical properties of the **CBP** derivatives by additional carbazole substituents. And indeed, optical and electrochemical analysis displayed that electron withdrawing CF_3-substituents (either in the 3,6-position in **3** or in the 2,7-position in **4**) stabilized the frontier orbitals, while electron donating CH_3O-substituents (in 2,7 position in **5**) increased the energy levels of the frontier orbitals. All new **CBP** derivatives displayed enhanced triplet energies compared to the parent **CBP** and DSC studies showed a long lasting amorphous states, emphasizing the application potential of these **CBP** derivatives as matrix material in blue emitting OLED's.

We are currently looking at alternative central motives of potential matrix materials as well as variations in the substitution patterns.

Supporting Information Available

Synthetic procedures and full characterization for all synthesized compounds, DSC traces, as well as gated steady state phosphorescence spectra for compounds **1-5** and x-ray structures for compounds **2**, **3** and **4** are provided as Supporting Information. This information is available free of charge via the Internet at http://pubs.acs.org/.

Acknowledgement

We thank the Swiss National Science Foundation and the University of Basel for financial support. This work has received funding from the European Union's Seventh Framework Program for research, technological development and demonstration under the ROSFEN project (grant agreement no. 312829).

Bibliography

(1) Tao, Y.; Yang, C.; Qin, J. *Chem. Soc. Rev.* **2011**, *40*, 2943–2970.

(2) Rotzler, J.; Gsellinger, H.; Bihlmeier, A.; Gantenbein, M.; Vonlanthen, D.; Häussinger, D.; Klopper, W.; Mayor, M. *Org. Biomol. Chem.* **2012**, *11*, 110–118.

(3) Sasabe, H.; Kido, J. *Eur. J. Org. Chem.* **2013**, *2013*, 7653–7663.

(4) Tanaka, I.; Tabata, Y.; Tokito, S. *Chem. Phys. Lett.* **2004**, *400*, 86–89.

(5) Schrögel, P.; Tomkevičienė, A.; Strohriegl, P.; Hoffmann, S. T.; Köhler, A.; Lennartz, C. *J. Mater. Chem.* **2011**, *21*, 2266.

(6) Schrögel, P.; Langer, N.; Schildknecht, C.; Wagenblast, G.; Lennartz, C.; Strohriegl, P. *Org. Electron.* **2011**, *12*, 2047–2055.

(7) Bedford, R. B.; Betham, M. *J. Org. Chem.* **2006**, *71*, 9403–9410.

(8) Watson, D. A.; Su, M.; Teverovskiy, G.; Zhang, Y.; García-Fortanet, J.; Kinzel, T.; Buchwald, S. L. *Science* **2009**, *325*, 1661–1664.

(9) Jian, H.; Tour, J. M. *J. Org. Chem.* **2003**, *68*, 5091–5103.

(10) Liou, G.-S.; Hsiao, S.-H.; Huang, N.-K.; Yang, Y.-L. *Macromolecules* **2006**, *39*, 5337–5346.

(11) Watanabe, M.; Nishiyama, M.; Yamamoto, T.; Koie, Y. *Tetrahedron Lett.* **2000**, *41*, 481–483.

(12) Sambiagio, C.; Marsden, S. P.; Blacker, A. J.; McGowan, P. C. *Chem. Soc. Rev.* **2014**, *43*, 3525–3550.

(13) Chen, Y.-C.; Huang, G.-S.; Hsiao, C.-C.; Chen, S.-A. *J. Am. Chem. Soc.* **2006**, *128*, 8549–8558.

(14) Kozaki, M.; Okada, K. *Org. Lett.* **2004**, *6*, 485–488.

(15) Zyryanov, G.; Kovalev, I.; Egorov, I.; Rusinov, V.; Chupakhin, O. *Chem. Heterocycl. Compd.* **2011**, *47*, 571–574.

(16) Wu, Q.; Wang, L. *Synthesis* **2008**, *2008*, 2007–2012.

(17) Krasovskiy, A.; Knochel, P. *Angew. Chem. Int. Ed.* **2004**, *43*, 3333–3336.

(18) Maji, M.; Studer, A. *Synthesis* **2009**, *2009*, 2467–2470.

(19) Tsang, W. C. P.; Munday, R. H.; Brasche, G.; Zheng, N.; Buchwald, S. L. *J. Org. Chem.* **2008**, *73*, 7603–7610.

(20) Kamino, B. A.; Mills, B.; Reali, C.; Gretton, M. J.; Brook, M. A.; Bender, T. P. *J. Org. Chem.* **2012**, *77*, 1663–1674.

(21) Krasnokutskaya, E.; Semenischeva, N.; Filimonov, V.; Knochel, P. *Synthesis* **2007**, *2007*, 81–84.

(22) Liu, C.-Y.; Gavryushin, A.; Knochel, P. *Chem. – Asian J.* **2007**, *2*, 1020–1030.

(23) Tsai, M.-H.; Hong, Y.-H.; Chang, C.-H.; Su, H.-C.; Wu, C.-C.; Matoliukstyte, A.; Simokaitiene, J.; Grigalevicius, S.; Grazulevicius, J. V.; Hsu, C.-P. *Adv. Mater.* **2007**, *19*, 862–866.

(24) Low, P. J.; Paterson, M. A. J.; Yufit, D. S.; Howard, J. A. K.; Cherryman, J. C.; Tackley, D. R.; Brook, R.; Brown, B. *J. Mater. Chem.* **2005**, *15*, 2304–2315.

(25) Deng, L.; Wang, X.; Zhang, Z.; Li, J. *J. Mater. Chem.* **2012**, *22*, 19700–19708.

(26) He, J.; Liu, H.; Dai, Y.; Ou, X.; Wang, J.; Tao, S.; Zhang, X.; Wang, P.; Ma, D. *J. Phys. Chem. C* **2009**, *113*, 6761–6767.

(27) Zotti, G.; Schiavon, G.; Zecchin, S.; Morin, J.-F.; Leclerc, M. *Macromolecules* **2002**, *35*, 2122–2128.

(28) Zheng, Y.; Batsanov, A. S.; Jankus, V.; Dias, F. B.; Bryce, M. R.; Monkman, A. P. *J. Org. Chem.* **2011**, *76*, 8300–8310.

(29) Haggquist, G. W.; Katayama, H.; Tsuchida, A.; Ito, S.; Yamamoto, M. *J. Phys. Chem.* **1993**, *97*, 9270–9273.
(30) Gomes, P. J. S.; Serpa, C.; Arnaut, L. G. *J. Photochem. Photobiol. Chem.* **2006**, *184*, 228–233.
(31) Cardona, C. M.; Li, W.; Kaifer, A. E.; Stockdale, D.; Bazan, G. C. *Adv. Mater.* **2011**, *23*, 2367–2371.
(32) Ambrose, J. F.; Nelson, R. F. *J. Electrochem. Soc.* **1968**, *115*, 1159–1164.

Table of Content Graphic:

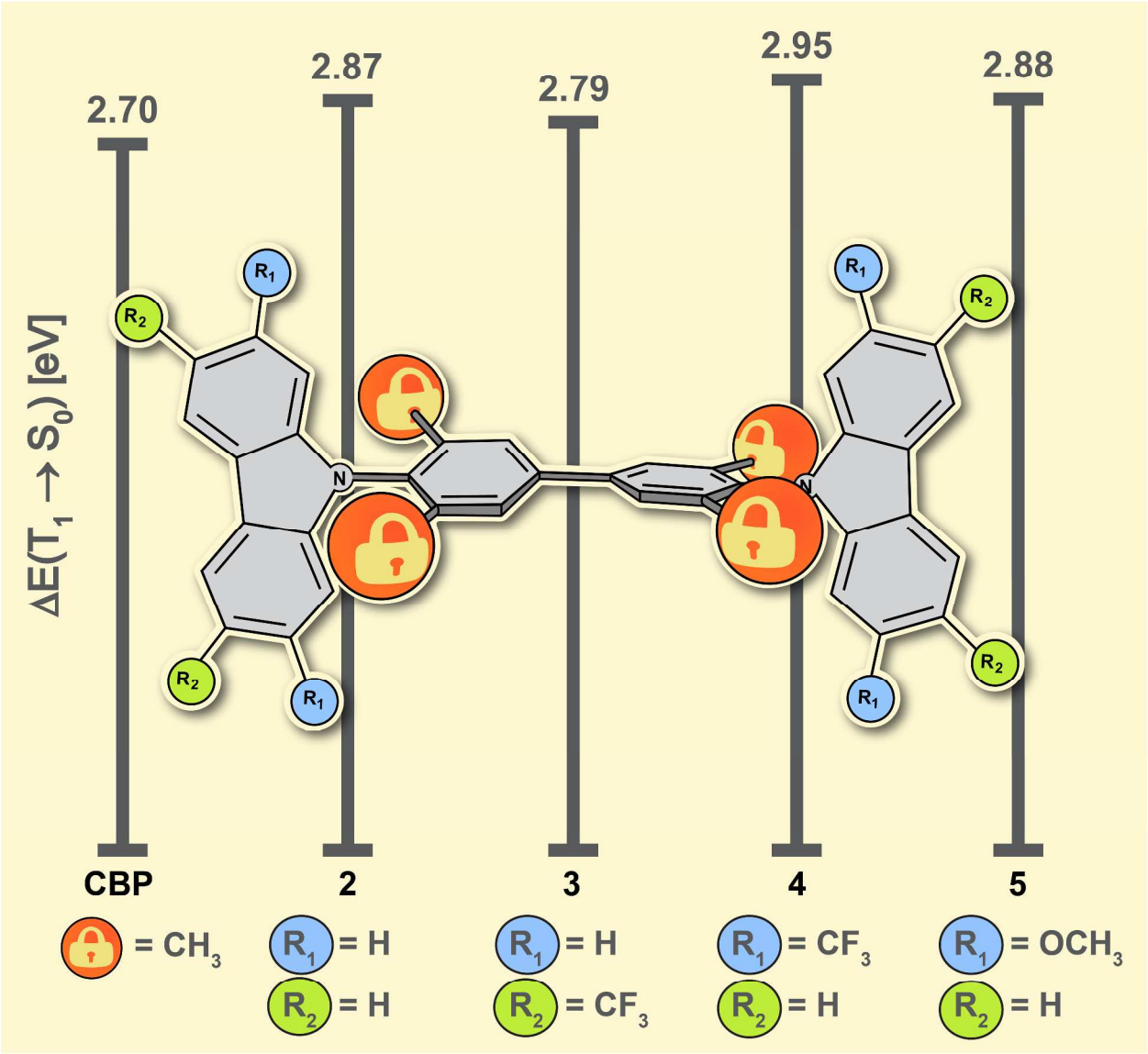

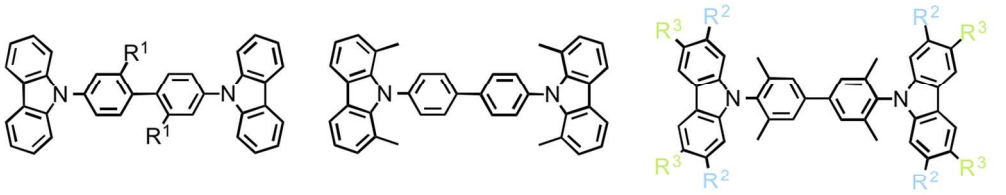

CBP: R^1 = H
CDBP: R^1 = CH_3

1

2: R^2 = R^3 = H
3: R^2 = **H**, R^3 = CF_3
4: R^2 = CF_3, R^3 = H
5: R^2 = OCH_3, R^3 = H

126x46mm (300 x 300 DPI)

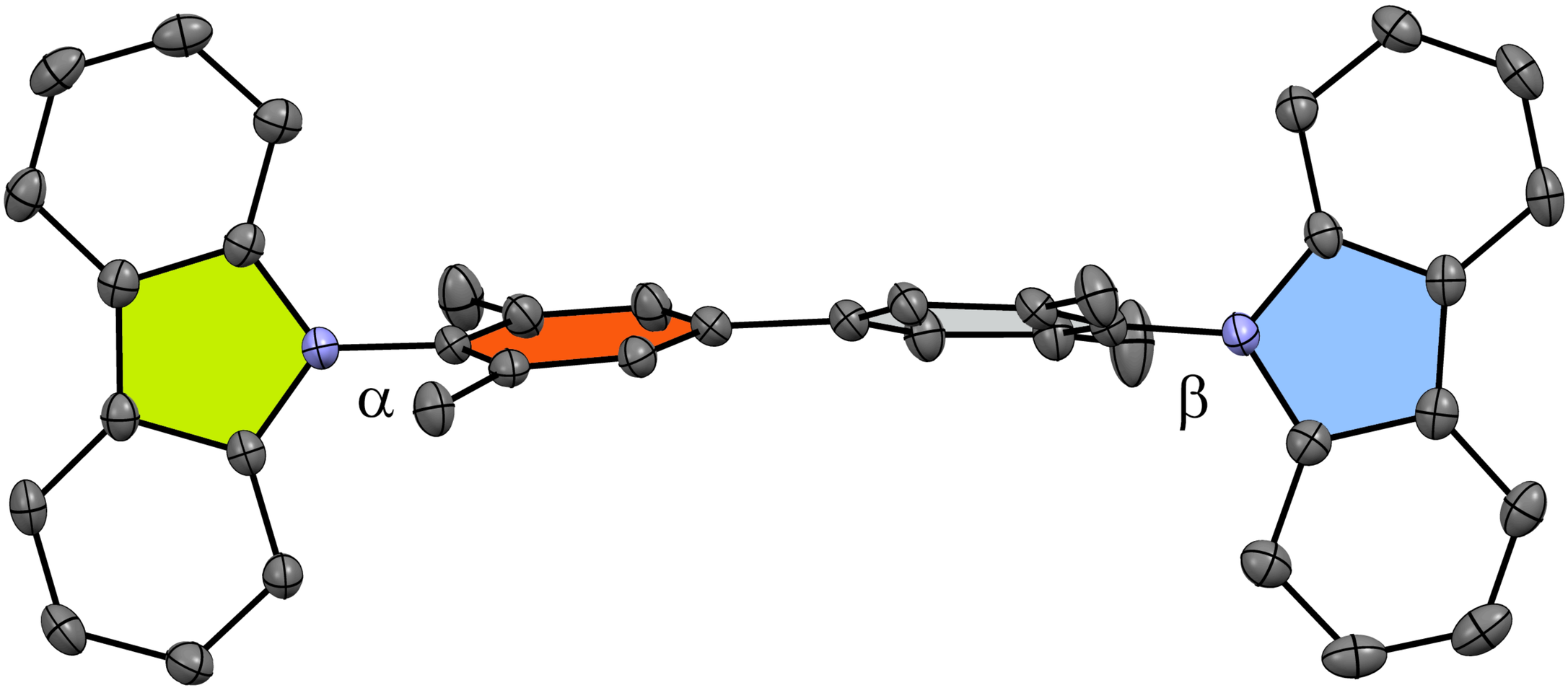
α
β

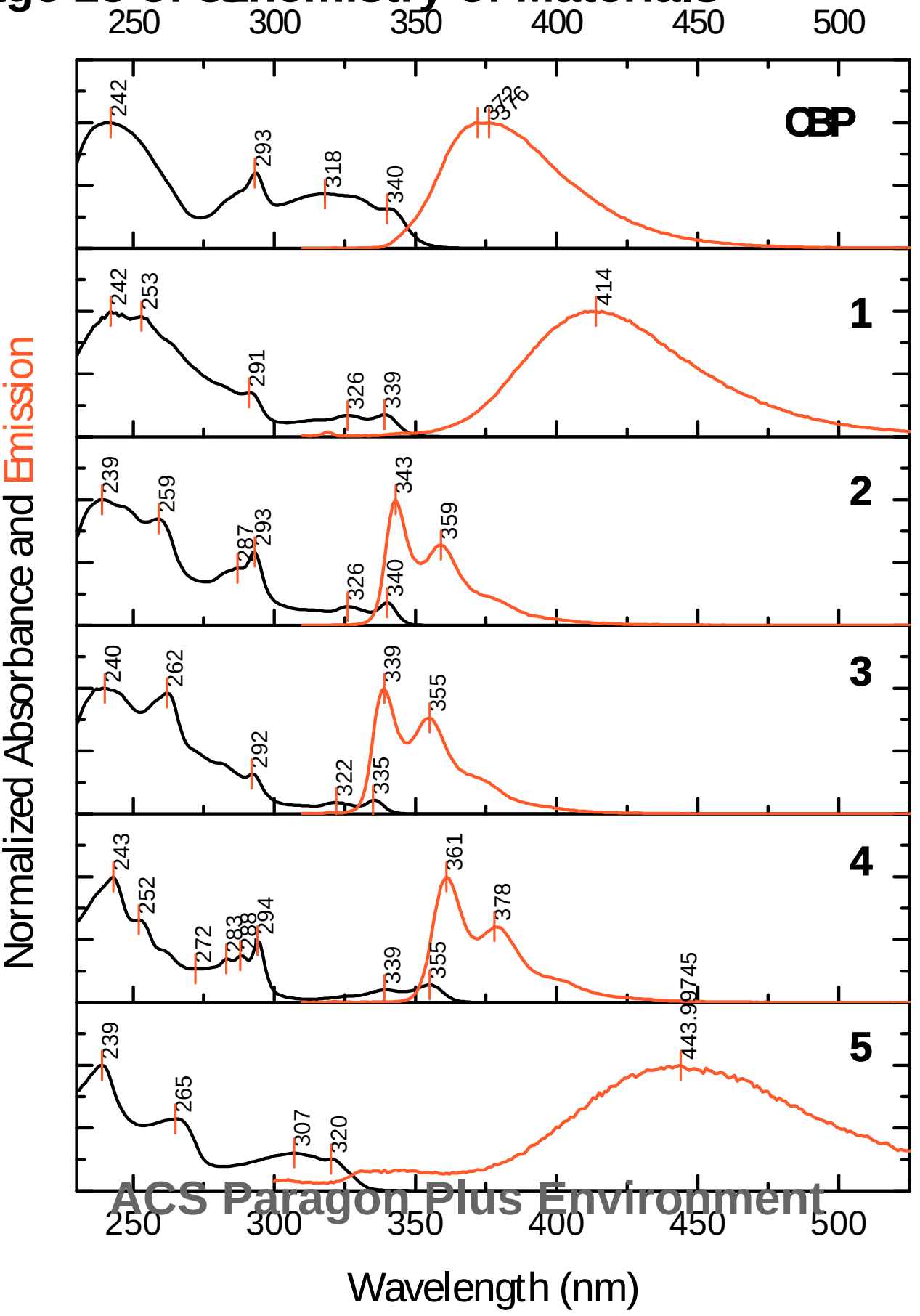

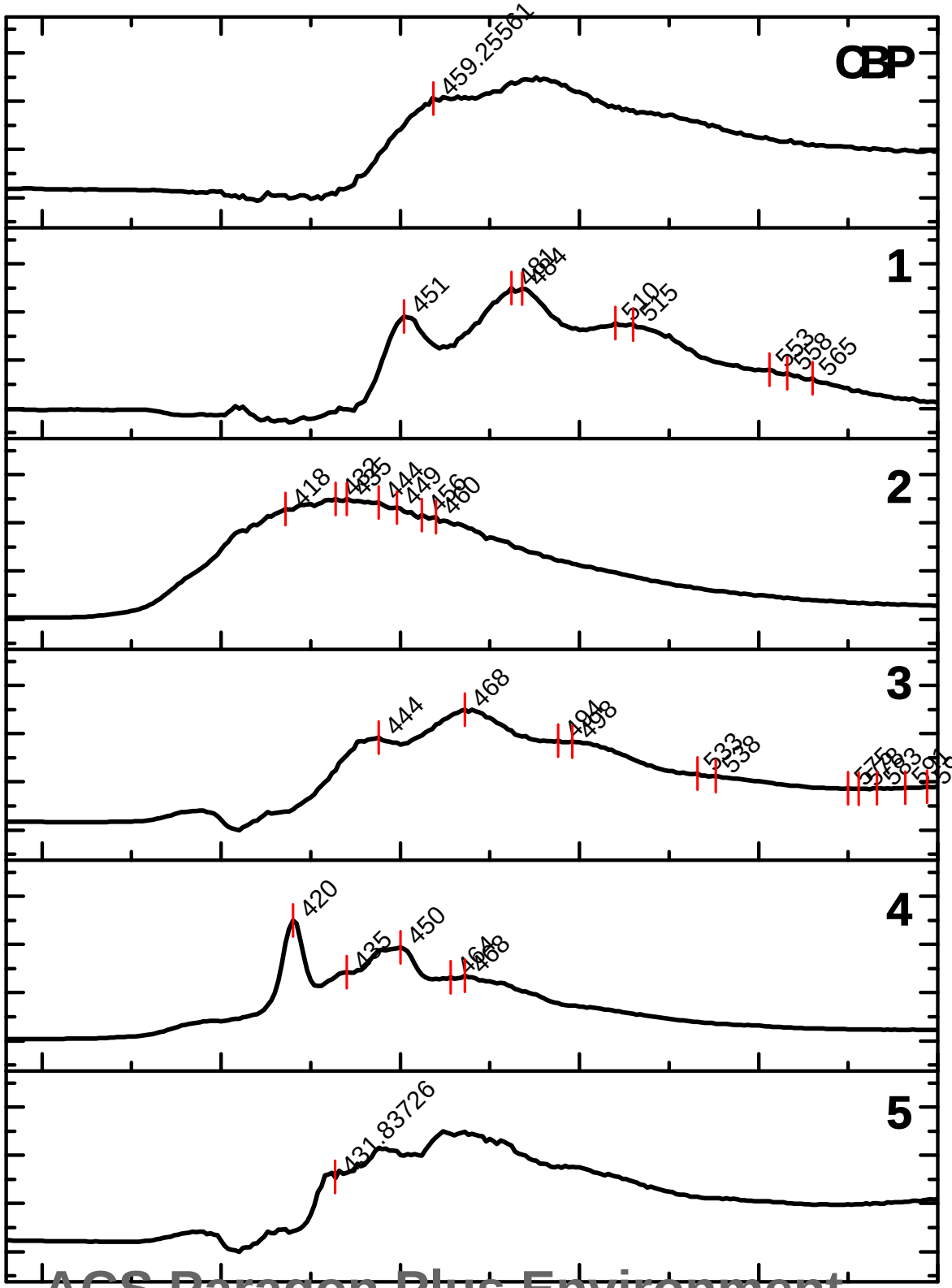

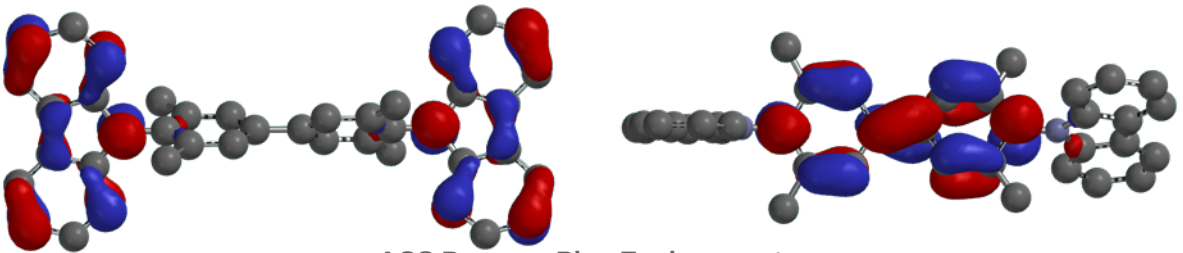

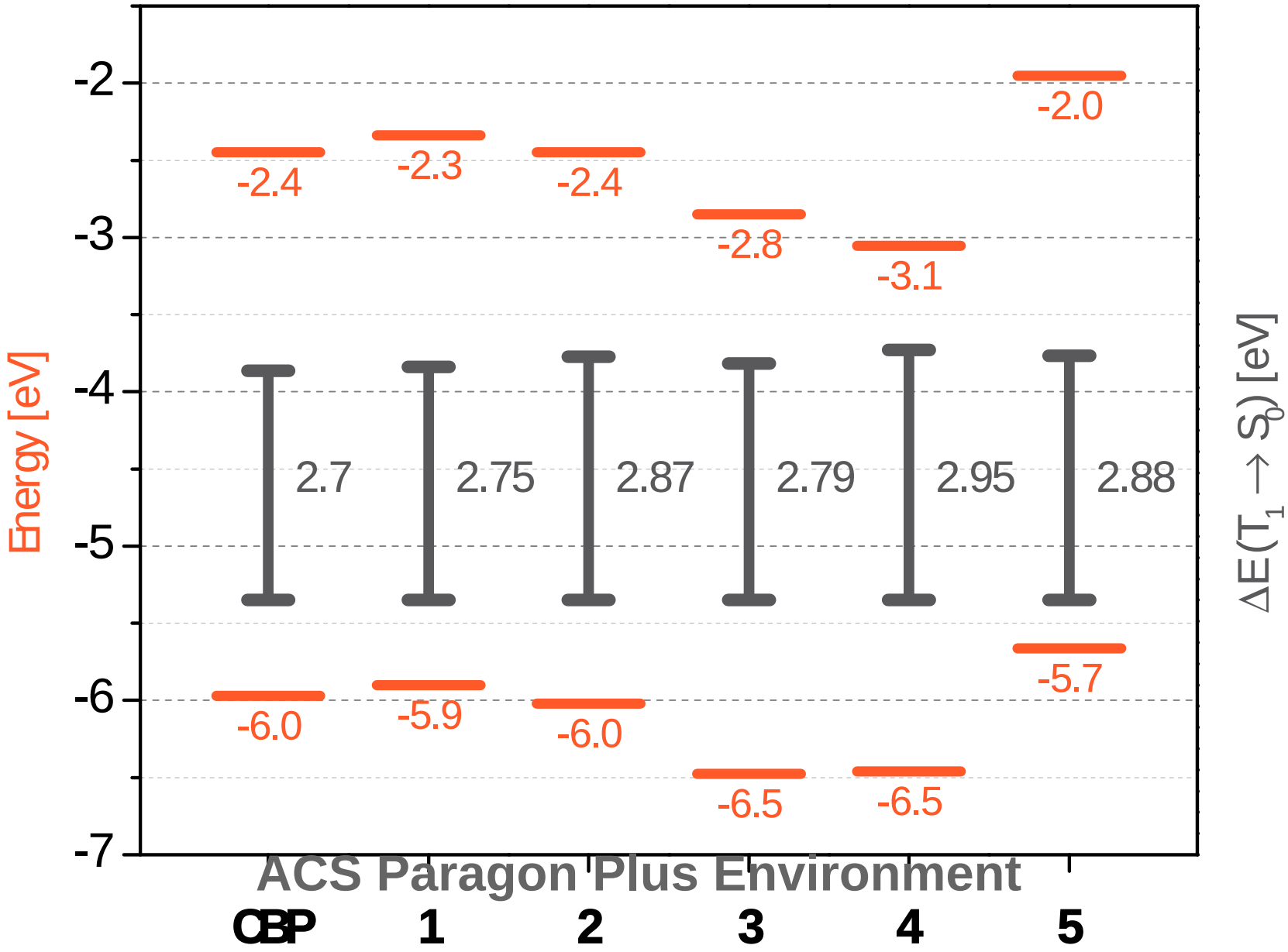
Energy [eV]
-2
-3
-4
-5
-6
-7
-2.4
-2.3
-2.4
-2.8
-3.1
-2.0
2.7
2.75
2.87
2.79
2.95
2.88
-6.0
-5.9
-6.0
-6.5
-6.5
-5.7
ΔE(T1 → S0) [eV]
ACS Paragon Plus Environment
CBP
1
2
3
4
5

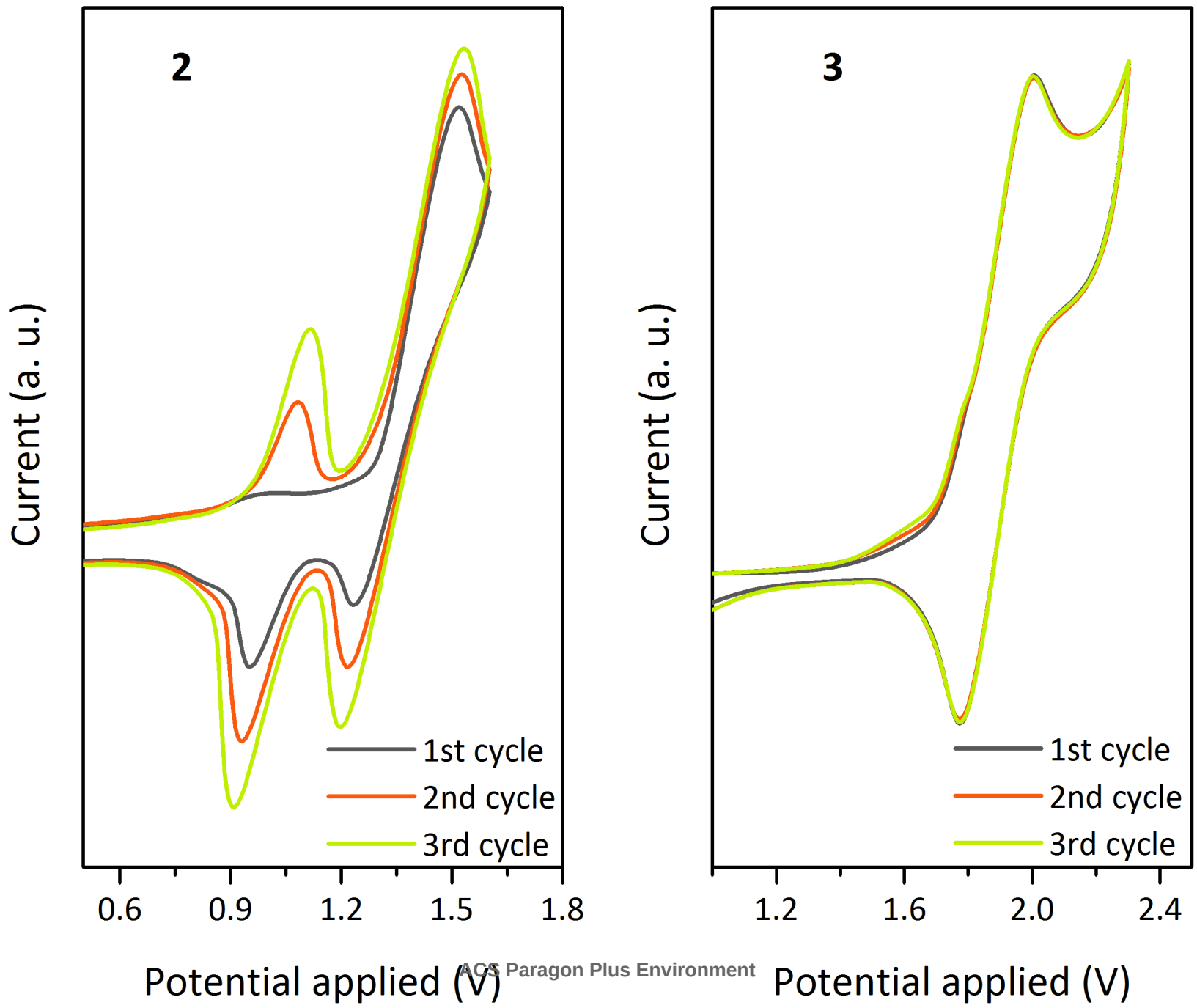

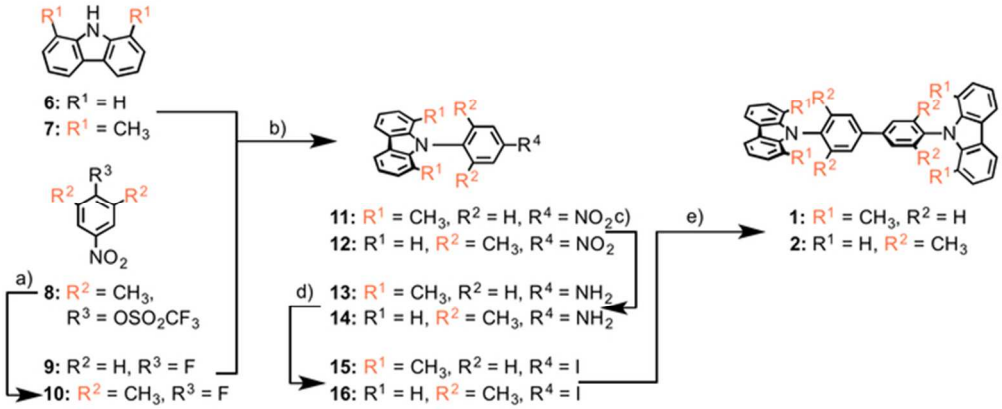

60x24mm (300 x 300 DPI)

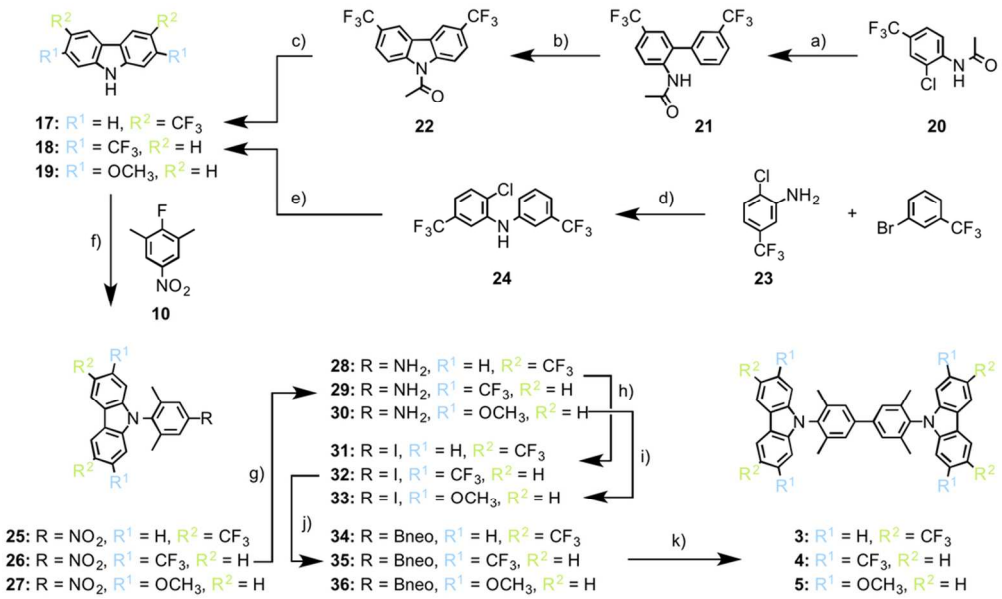

97x57mm (300 x 300 DPI)

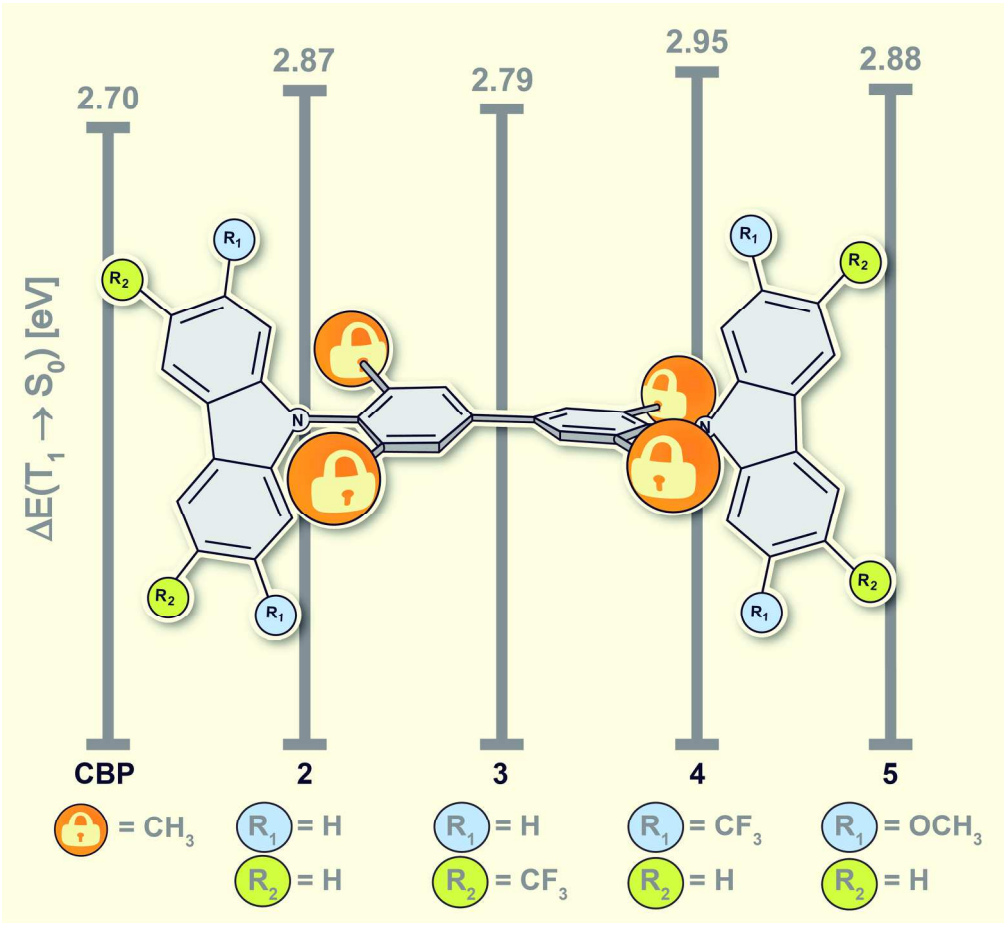

200x184mm (300 x 300 DPI)